PHYSICAL REVIEW C, VOLUME 62, 031603(R)

# Neutron-proton asymmetry of the midvelocity material in an intermediate-energy heavy-ion collision

L. G. Sobotka,[1] R. J. Charity,[1] D. K. Agnihotri,[2] W. Gawlikowicz,[2] T. X. Liu,[3] W. Lynch,[3] U. Schröder,[2] J. Tõke,[2] and H. S. Xu[3]

[1]*Department of Chemistry, Washington University, St. Louis, Missouri 63130*

[2]*Department of Chemistry, University of Rochester, Rochester, New York 14627*

[3]*Department of Physics and the National Superconducting Cyclotron Laboratory, Michigan State University, East Lansing, Michigan 48824*

(Received 27 March 2000; published 21 August 2000)

The *n-p* asymmetry of the material found in the midvelocity or ''neck'' region of an intermediate energy heavy-ion reaction is determined. In order to accomplish this task, data from two different experiments are utilized. While the *n-p* asymmetry of the light particles ($Z \leqslant 2$) is enriched in neutrons relative to the bulk matter, the total material found at midrapidity has an asymmetry indistinguishable from that of the entire system.

PACS number(s): 25.70.Mn, 25.70.Lm, 25.70.Pq

Previous work by us [1,2] and the INDRA Collaboration [3] indicates that light charged particles in the intermediate-velocity region of peripheral to midcentral heavy-ion collisions are neutron rich relative to those fragments found in the velocity regions associated with the projectile and target-like fragments. This apparent neutron enrichment in the central region might be due to one or more of the following.

(1) The influence of clustering, which can have the effect of amplifying a slight overall neutron enrichment of a system into a stronger neutron enrichment of the light ejectiles.

(2) A consequence of a Coulomb suppression of the more highly charged species and the action of sequential decay.

(3) An isospin-asymmetric migration of neutrons and protons between the low-density ''neck'' domain and the more dense adjacent matter.

The last of these potential explanations is the most interesting in that the process it considers could be understood as an equilibrium isospin fractionation effect between regions of different density [4–6]. Specifically, this equilibration process, unlike the other potential explanations, would tend to increase the neutron excess of the low-density (surface-like) ''neck'' region at the expense of the more dense adjacent matter in the projectile and targetlike remnants. This Rapid Communication seeks to answer the question of whether in fact the total $n/p$ ratio of the midvelocity region is different than that of the bulk system.

To date, charged-particle data have been presented for a number of systems at several energies. By far the most complete data have been collected by the INDRA Collaboration for the $^{129}$Xe+$^{nat}$Sn system between 25–50 MeV/nucleon [3,7]. This previous study decomposes the charged-particle yield into components attributable to (i) evaporation from the target and projectilelike sources and (ii) a midvelocity source. This previous study lacks information on the free neutrons and on the isotopic characteristics of the intermediate mass fragments (IMF's). The present Rapid Communication aims to fill these gaps and presents new results on the $^{129}$Xe+$^{120}$Sn reaction at $E/A=40$ MeV, which together with those from the INDRA study allow us to deduce the composition of the midvelocity material. The INDRA data set includes a study at 39 MeV/nucleon [7]. There is no reason to believe the slight difference in energy or the isotope mix (in the INDRA target) are differences of consequence. Nevertheless, care must be taken to ensure that data sets from the two experiments span similar impact parameter ranges.

Acquiring data on neutron emission patterns of a quality that allows for a source decomposition analysis, requires excess scattering material be kept to a minimum. Therefore such data cannot be reliably collected in the same experiment as one which characterizes the charged-particle emission patterns with a $4\pi$ detector. As a result, common impact-parameter selectors cannot be used. However as we desire to compare to the peripheral or mid central data from INDRA, some impact-parameter selection must be provided. In order to accomplish this we have measured both the charge of the projectilelike fragment ($Z_{\mathrm{PLF}}$) and $\alpha$-particle spectra. (Some limited data were also collected for the IMF's.) Previous work [2] indicates that the charge of the projectilelike fragment $Z_{\mathrm{PLF}}$ is inversely related to the average charged-particle multiplicity and thus can be used as a measure of centrality. In the present Rapid Communication we select events by requiring that a projectilelike fragment of $15< Z_{\mathrm{PLF}}<35$ be detected just beyond the grazing angle. This kind of gating condition filters out the most central collisions, for which no large projectile remnant remains, and the most peripheral ones, characterized by very moderate charged particle evaporation from projectilelike fragments (PLF's). However such a selection is rather crude and we have, *a priori*, no knowledge of the actual impact-parameter window selected. On the other hand, the $\alpha$-particle data can be compared to those collected with $4\pi$ detectors to provide a fix on the impact-parameter region selected.

Projectilelike fragments (PLF's) were detected between 4.6° and 9.3° with an annular Si-CsI(Tl) array. This telescope provided the atomic number and energy of the PLF's. Four charged-particle telescopes, consisting of two Si layers backed by CsI(Tl), were used to detect $\alpha$ particles. Each of the Si layers consist of $50\times50$ mm, 16-strip devices. The

 

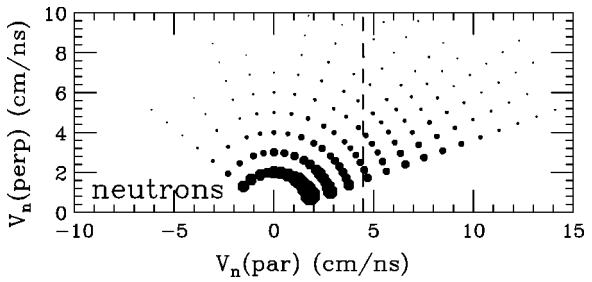


FIG. 1. Invariant neutron cross section plot for the system $E/A=40$ MeV $^{129}$Xe+$^{120}$Sn when PLF's are detected just beyond the grazing angle. The area of the plotted symbols is proportional to the cross section. The dashed line indicates the center-of-mass velocity.

first is 65 $\mu$m thick and the second (orthogonally oriented) is 1000 $\mu$m thick. Four 2 cm thick CsI(Tl) detectors were positioned, in a quadrant arrangement, behind the Si detectors. This thickness is sufficient to stop all of the $\alpha$ particles but insufficient to stop the hydrogen isotopes. The telescopes were run at two sets of angles. For analysis purposes the angles were defined by the CsI(Tl) positions thus data were obtained at 16 polar angles. These telescopes were calibrated with $\alpha$-particle and deuteron elastic scattering at small angles. The charged-particle detectors, along with two CsF scintillators were positioned inside of a thin walled (3.2 mm) Al scattering chamber of 80 cm diameter.

Neutron time-of-flight spectra were measured with a set of 15 discrete BC501A scintillator detectors (7.6 cm thick and 11.4 cm in diameter). These detectors varied in distance from the target from 2472 to 1045 mm, forward to backward angles, respectively. The *n* detectors were used in conjunction with plastic paddles positioned in front of the *n* detectors and the two small (20mm$\times$40 mm) CsF detectors positioned close to the target. The former were used to veto charged particles which penetrated the vacuum vessel and the latter provided the start for the time-of-flight measurement. The overall time resolution as determined from the $\gamma$-ray flash was 2.1 ns (FWHM). The efficiencies of the *n* detectors were calculated with the code SCINFUL [8]. The low-energy efficiency was verified via a calibration with $^{252}$Cf [9]. Software thresholds were set at 200 keeV.

Charged-particle invariant cross section maps for the Xe + Sn system have been presented in [3]. Figure 1 provides the neutron invariant cross section map for the system and event selection of the present Rapid Communication. Due to the absence of Coulomb rings, the source patterns are not apparent. Nevertheless, source fits clearly indicate the need for multiple sources.

A parametrization assuming an emission scenario with three moving sources, projectilelike, targetlike, and midvelocity, was used to obtain fits to both the neutron and $\alpha$-particle data. In the fit to the $\alpha$-particle data, all the multiplicities and temperatures were allowed to vary. The velocities of the projectilelike and targetlike sources were also allowed to vary. The midvelocity source was fixed at the center-of-mass velocity and the Coulomb barriers were fixed at 8 MeV for the target and projectile sources. A Gaussian

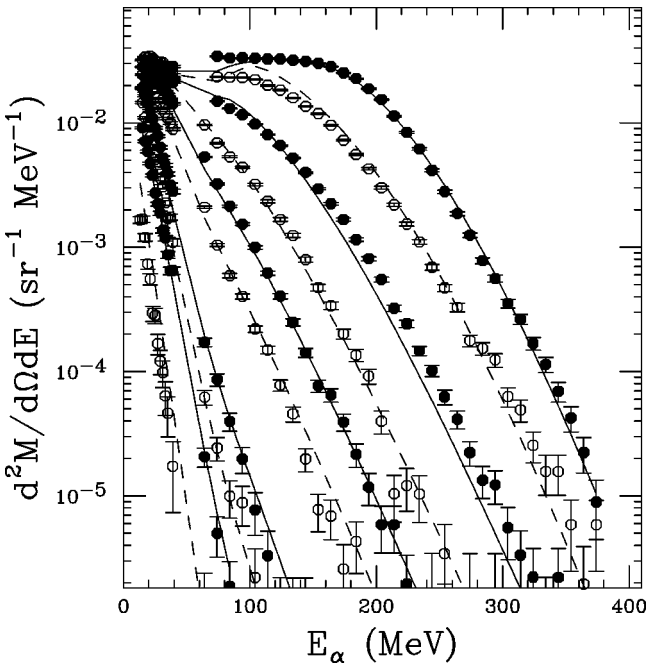


FIG. 2. Displayed are the $\alpha$-particle data at $\Theta_{lab}=16°$, 23°, 33°, 45°, 55°, 64°, 85°, 95°, 105°, and 154° (top to bottom) as well as the fit using a three source model. Data from additional angles are suppressed to improve figure clarity.

variation of the Coulomb barriers with a standard deviation of 50% of the mean was also included. The projectile and targetlike sources were taken to be of the surface type while a volume type was used for the midvelocity source. The large variation of the Coulomb barrier is needed to reproduce the data and the magnitude of the variation is similar to that needed previously when a similar procedure was used for fitting the charged particle data from an intermediate-energy heavy-ion reaction [10]. In fitting the neutron data, the sources were modeled with relativistic Maxwell-Boltzmann distributions folded with a resolution function (derived from a Gaussian distribution in time) and the projectile and targetlike source velocities were fixed at the values extracted from the fit to the $\alpha$-particle data. The fit to the $\alpha$-particle data, shown in Fig. 2, represents the data very well while that for the neutron data, shown in Fig. 3, suggests the need for additional forward and backward components, each with small multiplicity.

The extracted multiplicities from the midvelocity source ($Mid$) and the sum of the targetlike and projectilelike sources ($T+P$) are shown in Fig. 4 as the ''birdlike'' symbols. The charged-particle data from INDRA are also shown for the four most peripheral bins reported by Plagnol *et al.* [7]. These charged particle data span from $b=10$ fm to $b=4$ fm (bins 1 through 4, respectively, see caption or Ref. [7]). Each element is presented as a different symbol and we have dispersed the data from the four bins by the addition of abscissa offsets which increase with increasing centrality. First we focus on the $\alpha$-particle data. Our data, in terms of both the (a) mid-velocity and (b) target + projectile multiplicities [and thus the ratio (c)] are very close to those extracted from the INDRA data for bins 3 and 4. These bins

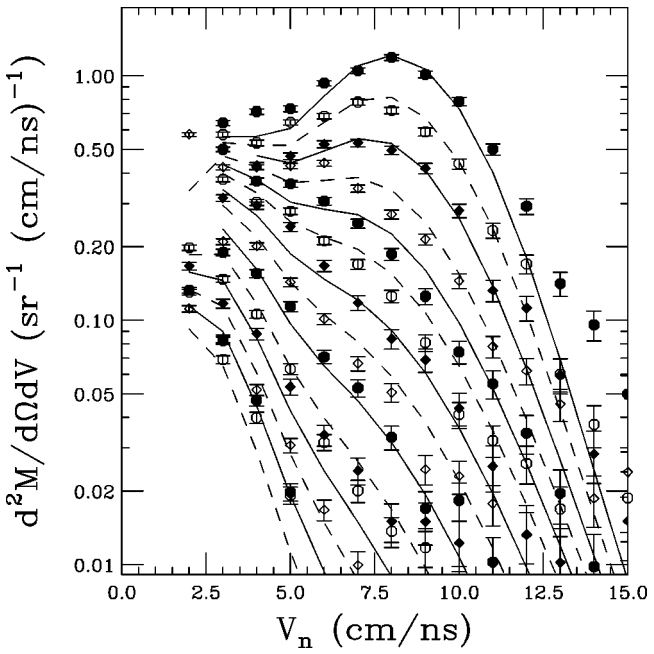


FIG. 3. Displayed are the neutron data from $\Theta_{lab}=20°$, 25°, 30°, 35°, 40°, 45°, 53°, 60°, 70°, 80°, 90°, 100°, 110°, and 125° (top to bottom) as well as the fit using a three source model. Data from additional angles are suppressed to aid figure clarity.

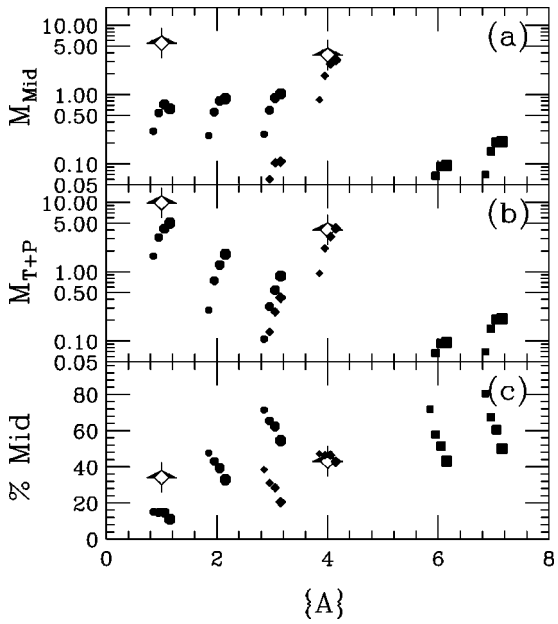


FIG. 4. The multiplicities of neutrons and charged particles from the midvelocity (a) and target and projectilelike sources (b) as well as the midvelocity fraction (c), are shown for $E/A=40$ MeV Xe+Sn. The neutron and alpha data from the present experiment are shown as the ''birdlike'' symbols. The charged-particle results from the four most peripheral bins of the INDRA study of the same system are also displayed. To better visualize the trends, the data points are dispersed about the actual atomic mass number left to right (smaller to larger symbols) with increasing centrality. These four bins (1–4) correspond to deduced impact-parameter selections of $10>b>8.5$, $8.5>b>7.0$, $7.0>b>5.5$, and $5.5>b>4.0$. Circles, diamonds, and squares are used to represent the data for atomic numbers 1, 2, and 3, respectively.

correspond to the impact-parameter window $4<b<7$ fm which is consistent with the expectation that the employed filter removes both the most central and peripheral events. Additional confidence that the data sets can be compared in this impact parameter interval comes from the extracted velocity of the PLF's. The fit to the $\alpha$-particle data yielded a projectile velocity of $\beta_{\mathrm{c.m.}}^{\mathrm{PLF}}=0.107$, a value close to that extracted from the $4\pi$ charged particle data for bin 4, $\beta_{\mathrm{c.m.}}^{\mathrm{PLF}}=0.111$ [11], suggesting that the mean impact parameter of the selected data is about 5 fm.

For this event selection, the neutron multiplicity is almost 10 times the proton multiplicity for the midvelocity yield, while it is only twice the proton multiplicity for the projectilelike and targetlike yields. While the fraction of neutrons emitted in the midvelocity region [see Fig. 4(c)] is substantially greater than that for protons, it is about equal to that for deuterons and $\alpha$ particles. Other trends which can be seen from this figure are the marked tendency for the heavier hydrogen isotopes and heavy clusters to be found at midvelocity. While these trends have been previously noted, another trend seen in this plot has not. There is a decrease in the relative emission of $d$, $t$, $^3$He, $^6$Li, and $^7$Li, at midvelocity with increasing centrality. While the magnitude of this trend may be influenced by the extraction procedure, it suggests that the emission mechanisms and/or the relative position on excitation functions, increasingly favor the emission of these particles from the target and projectilelike sources as the centrality increases.

While the INDRA data provide an estimate of the IMF multiplicity, the isotope composition was not determined for these fragments. The charge particle detectors used in the present Rapid Communication do provide this information up to $Z=6$, albeit (in this experiment) with insufficient granularity at forward angles to allow for an IMF source decomposition analysis. Figure 5 shows an example of a particle-identification (PID) spectrum at a laboratory angle of 25°. Assuming that the IMF's detected at this angle are representative of the midvelocity source, we find that the mean values of $(N/Z)$ are 1.18, 1.02, 1.32, 1.26, 1.23, and 1.13 for $Z=1$, 2, 3, 4, 5, and 6, respectively.

The measured multiplicities and values of $(N/Z)$ allow us to estimate the composition of the material found at midvelocity as well as determine the overall charge partition of the selected events. The particle tally is presented in Table I. The multiplicity of the charged particles is taken from Ref. [7] (bin 4) except for $\alpha$-particles for which the average of the multiplicity of the present Rapid Communication and that of Ref. [7] was used. The bulk of the charge resides in the projectilelike (detected) and targetlike (inferred) residues. The average value of the PLF charge is $\langle Z_{\mathrm{PLF}}\rangle=25.2$. As the system is nearly symmetric, the mean value of $Z_{\mathrm{TLF}}$ must be similar. With this inference we account for just over 90% of the charge of the system, about 1/2 of which is contained in the two heavy residues. Of the remainder, about 3/5 ($\sim$30 units) is evaporated from the target and projectilelike fragments and 2/5 ($\sim$20 units) comprise the midvelocity source.

Using the measured multiplicities for the isotopically re-

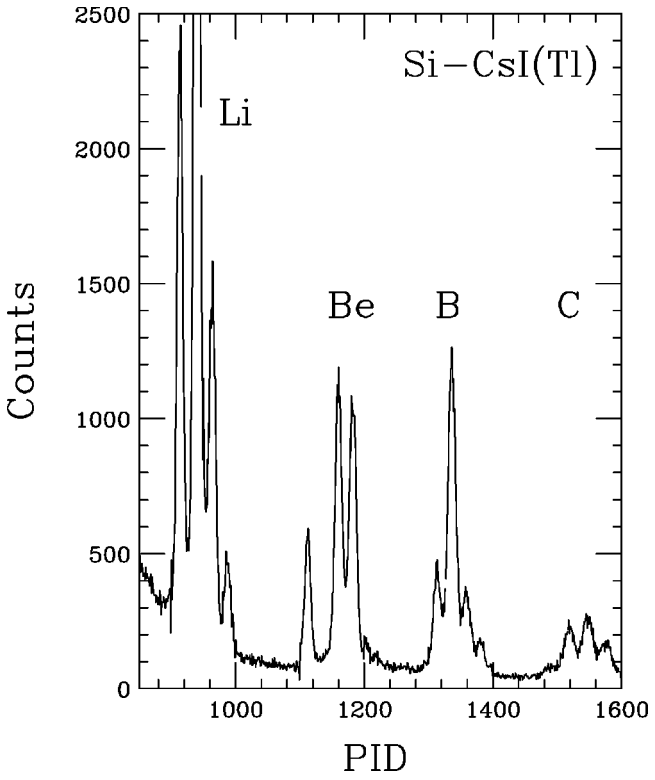


FIG. 5. Particle-identification spectrum from a detector at $\Theta_{lab} = 25°$ using the Si-CsI(Tl) pulse heights. The C data are underrepresented in this plot as many of these fragments are stopped in the second Si telescope element.

solved light ions, the measured IMF multiplicity (from INDRA), and mean IMF $N/Z$ ratio for $Z \leqslant 6$ (present experiment), we find that the midvelocity source is of modest mean size ($\sim 47$ nucleons) with $(N/Z)_{Mid} = 1.38 \pm 0.07$. The latter value is indistinguishable from that of the bulk system $(N/Z)_{sys} = 1.394$. On the other hand a value of $(N/Z) = 1.4$ is neutron rich relative to $\beta$ stability for a system of the size of the midvelocity source. If one does not include the IMF's in the particle tally, the extracted value of $(N/Z)_{Mid}$ is 1.65 and if only the fragments with $Z \leqslant 6$ are included in the tally (those for which isotope information is available) the value of $(N/Z)_{Mid}$ is 1.51. The quoted uncertainly on the value of $(N/Z)_{Mid}$ comes from making extreme assumptions concerning the value of $N/Z$ for the (heavier) isotopically unresolved IMF's.

TABLE I. Particle tally.

| | $n$ | H | He | IMF | Heaviest | Total |
|---|---|---|---|---|---|---|
| $M_{Mid}$ | 5.5 | 2.6 | 3.5 | 2.0 | | 13.6 |
| $Z_{Mid}$ | 0 | 2.6 | 7.0 | $\sim 10$ | | 20 |
| $A_{Mid}$ | 5.5 | 5.7 | 14.1 | 22 | | 47 |
| $(N/Z)_{Mid}$ | | 1.18 | 1.02 | $\sim 1.2$ | | 1.4 |
| $M_{TP}$ | 11.3 | 7.7 | 4.7 | 2 | 2 | 28 |
| $Z_{TP}$ | 0 | 7.7 | 9.4 | $\sim 10$ | $\sim 48$ | 75 |
| $(N/Z)_{TP}$ | | 0.46 | 0.97 | | | |

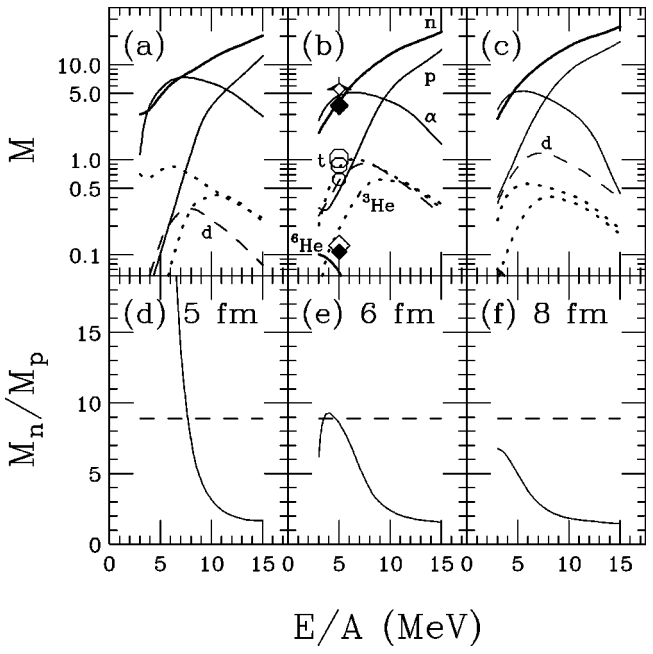


FIG. 6. Results of microcanonical calculations for 46 nucleons, 19 protons, and 27 neutrons in volumes equal to that of spheres of radii 5 (first column), 6 (middle column), and 8 fm (last column). Fragments with $Z \leqslant 4$ and $A \leqslant 10$ are explicitly considered in this calculation. In sections (a)–(c) $n$, $p$, and $\alpha$ particles are represented by solid lines, $d$ by the dashed lines, and $t$ and $^3$He by dotted lines. The neutron multiplicity is always the largest while for the charged particles, $\alpha$ particles (protons) are the most prevalent at low (high) energies. The experimental data for $Z = 0$, 1, and 2 are displayed in section (b) as the birdlike, circle, and diamond symbols, respectively. (The open diamond and solid line in the lower left are the data and calculations for $^6$He.) The larger the symbol the heavier the isotope. Sections (d)–(f) provide the calculated (solid) and experimental (dashed horizontal) free $n/p$ ratio. The excluded volumes for the light ions are calculated with the following radii: 0.8, 0.8, 2.2, 1.9, 1.9, and 1.6 fm for $n$, $p$, $d$, $t$, $^3$He, and $\alpha$ particles, respectively. A radius parameter of 1.4 fm was used for the heavier clusters.

An understanding of this intermediate-velocity zone clearly requires a dynamical model which treats clusters. Nevertheless useful insight can be gained from schematic equilibrium-statistical calculations. Figure 6 presents the results of a microcanonical calculation which considers all partitions of 46 nucleons, 27 neutrons, and 19 protons, into fragments with $Z \leqslant 4$ and $A \leqslant 10$. In addition to the ground states, 13 low-lying excited states for the IMF's, both bound and unbound, are explicitly considered. To account for the heavier IMF's, not explicitly considered, a pseudo heavy IMF is included with the correct value of $(N/Z)$ and a degeneracy adjusted to reproduce the experimental multiplicity of fragments with $Z > 4$ [12]. This calculation makes use of the techniques described by Randrup [13] to evaluate the phase space integrals for each partition. The reason we have followed a procedure by which all partitions must be included in an enumeration is that it readily allows us to explicitly consider excluded volume effects. Specifically we exclude volumes consistent with wave function sizes (see

figure caption). The expected multiplicities (top sections) and the free $n/p$ ratio (bottom sections) are shown for three different densities [roughly 0.55, 0.32, and 0.13 of the saturation density, sections (a),(d); (b),(e); and (c),(f), respectively].

The striking trend seen in Fig. 6 is the sensitivity of the deuteron yield (dashed line) to the confining volume. For the smaller volume (a), the deuteron yield is substantially below that of tritons over the entire energy range. The low yield of deuterons is attributable to both the small binding energy of deuterons and their disproportionately large size. When the volume is increased to that of a sphere of 8 fm [section (c)] the large size of the deuteron is of lesser consequence, allowing the yield to increase. Providing the fragment production proceeds according to the direct and sequential decay channels considered in this equilibrium-statistical model, our results illustrate that the deuteron yield should be a sensitive indicator of the density at breakup. The experimental data are shown as solid symbols (b) at a value of the energy per nucleon for which there is a favorable comparison between the data and calculations. At this low energy ($E/A \sim 5$ MeV) about 75% of the matter is in well bound fragments, the hydrogen isotopes all have about the same yield, and the $n/p$ and $t/^3$He ratios are about 11 and 6, respectively. These simple calculations indicate that the observed large mass fraction in well bound fragments and the large $n/p$ and $t/^3$He ratios, on the one hand and significant $d$ yields on the other, are the equilibrium expectations for a rather modestly excited and dilute system, respectively. It is also worth noting that this excitation energy ($E/A \sim 5$ MeV) is consistent with the fit temperature values for the midrapidity source ($6.3 \pm 0.9$ MeV for neutrons) assuming standard values of the Fermi-gas level density parameter.

The influence of sequential decay varies from small for the nucleons to modest for deuterons, where the yield is increased a factor of $\sim 2$, to quite large for $\alpha$ particles for which sequential decay increases the yield by a factor of $\sim 4$. Clearly the agreement between the experimental yields and this model calculation could not be achieved without the inclusion of the prominent decay channels.

In summary, our results indicate that the $N/Z$ ratio of the material found at the midvelocity region is the same as the $N/Z$ ratio of the bulk matter. Model calculations suggest that the light fragment composition is roughly what one would expect from an equilibrium partition of a system of the correct total nucleon and isospin composition if the partitioning occurs at low density and with an energy per nucleon similar to, but not exceeding, the saturation value of the binding energy per nucleon. As a result of these findings we conclude that the large $n/p$ and $t/^3$He ratios found in the midvelocity region (relative to those found in the target and projectile-like velocity regions) are a result of the large fraction of matter in well-bound nearly symmetrical clusters and the relative $n$-enrichment of the rather modest-sized midvelocity source. While the present Rapid Communication utilizes a tractable equilibrium calculation (with sequential decay), it is also possible that any model with the correct system size and $N/Z$ ratio which incorporates the basic physics which tends to produce fragments on the evaporation attractor line [14] could also reproduce the fragment yields.

We would like to thank Dr. E. Plagnol and Dr. A. Chbihi for providing the INDRA results in tabular form and Professor A. Galonsky for the loan of his neutron detectors. This work was supported by the U.S. Department of Energy under Grant Nos. DE-FG02-87ER40316 (Washington University) and DE-FG02-88ER40414 (University of Rochester) and by the National Science Foundation under Grant No. PHY-940366.

[1] J. T̃oke *et al.*, Phys. Rev. Lett. **75**, 2920 (1995).
[2] J.F. Dempsey *et al.*, Phys. Rev. C **54**, 1710 (1996).
[3] J. Łukasik *et al.*, INDRA Collaboration, Phys. Rev. C **55**, 1906 (1997).
[4] M. Barranco and J.R. Buchler, Phys. Rev. C **22**, 1729 (1980).
[5] N.K. Glendenning, Phys. Rev. D **46**, 1274 (1992).
[6] H. Müller and B.D. Serot, Phys. Rev. C **52**, 2072 (1995).
[7] E. Plagnol *et al.*, INDRA Collaboration, Phys. Rev. C **61**, 014606 (2000).
[8] J.K. Dickens, computer code SCINFUL, ORNL-6462 (1988), NEA Data Bank Program: PSR-0267 (1994). This code underpredicts the low energy response by about 10%. The efficiencies from the code were used in this work.
[9] C. Wagemans, *The Nuclear Fission Process* (CRC, Boca Raton, 1991), Chap. 11.
[10] D.J. Fields *et al.*, Phys. Rev. C **34**, 536 (1986).
[11] These velocities (as well as the multiplicities for the charged particles used in this work) are those from method (I) [7].
[12] This adjustment is done around $E/A$ (MeV) $\sim 5$.
[13] J. Randrup, Comput. Phys. Commun. **59**, 439 (1990). The momentum-space integral is evaluated under the sole constraint of energy conservation. The volume of each particle in the configuration is removed from the total volume to generate the free volume used for the position-space contribution of phase space.
[14] R.J. Charity, Phys. Rev. C **58**, 1073 (1998).